ACS APPLIED MATERIALS & INTERFACES

Research Article

www.acsami.org

Extrusion of Polysaccharide Nanocrystal Reinforced Polymer Nanocomposites through Compatibilization with Poly(ethylene oxide)

Mariana Pereda,[†,‡] Nadia El Kissi,[‡] and Alain Dufresne*[,†]

[†]The International School of Paper, Print Media and Biomaterials (Pagora), Grenoble Institute of Technology (Grenoble INP), CS10065, 38402 Saint Martin d'Hères Cedex, France

[‡]Laboratoire Rhéologie et Procédés, Grenoble INP-CNRS-UJF, UMR 5520, BP 53, 38041 Grenoble Cedex 9, France

Supporting Information

ABSTRACT: Polysaccharide nanocrystals with a rodlike shape but with different dimensions and specific surface area were prepared from cotton and capim dourado cellulose, and with a plateletlike morphology from waxy maize starch granules. The rheological behavior of aqueous solutions of poly(ethylene oxide) (PEO) with different molecular weights when adding these nanoparticles was investigated evidencing specific interactions between PEO chains and nanocrystals. Because PEO also bears hydrophobic moieties, it was employed as a compatibilizing agent for the melt processing of polymer nanocomposites. The freeze-dried mixtures were used to prepare nanocomposite materials with a low density polyethylene matrix by extrusion. The thermal and mechanical behavior of ensuing nanocomposites was studied.

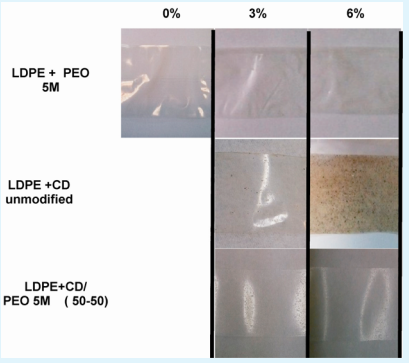

KEYWORDS: *cellulose nanocrystal, starch nanocrystal, nanocomposite, melt processing, extrusion*

INTRODUCTION

A flourishing and abundant literature devoted to cellulosic nanoparticles has emerged in recent years. Many works and reviews have been reported on the use of these nanoparticles as promising candidates for the reinforcement of polymer matrices.[1−5] Some significant technological challenges have been overcome. One of these is the existence of facilities for industrial-scale production of cellulose nanocrystals (CNCs). Most studies focus on their mechanical properties as reinforcing phase for polymers because of the inherent structural nature of cellulose.

However, a crucial step is obviously the processing of nanocomposites. Both CNCs and cellulose nanofibrils occur as aqueous suspensions after chemical or mechanical treatment, respectively, of the biomass. Because of the good dispersion level of cellulose nanoparticles in water, it is obviously the most suitable processing medium. Both water-soluble polymers and polymer aqueous dispersions (latex) have been extensively used.[6−10] After mixing the cellulose nanoparticle dispersion with the polymer solution/dispersion, a solid nanocomposite film can be obtained by simple casting and water evaporation. This mode of processing allows preserving the individualization state of the nanoparticles resulting from their colloidal dispersion in water.

Stable suspensions of CNCs with negatively charged surface groups, commonly produced by hydrolysis of the native cellulose with sulfuric acid, can be obtained in various polar liquid media broadening the range of polymer matrices.[11−13] Casting from a mixture of solvents can also be used to prepare cellulose nanoparticle-reinforced nanocomposites. By this method, the aqueous suspension of nanoparticles is mixed with a polymer solution involving a solvent miscible with water, e.g. tetrahydrofuran (THF).[14] Solvent exchange procedure can be used to suspend cellulosic nanoparticles in the proper liquid medium for further surface chemical modification, or mixing with a polymer solution or monomer for subsequent in situ polymerization.[15] Another approach involving a solvent exchange procedure and consisting in forming a network of CNC through a sol−gel process that subsequently serves as a template that can be filled with a polymer was also investigated.[16]

Stable cellulose nanoparticle dispersions in apolar or low polarity solvent can be obtained by physically coating their surface with a surfactant[17] or chemically grafting apolar moieties onto their surface.[18] Both methods allow tuning the surface and decreasing the surface energy of the nanoparticle.

The previous processing techniques used a liquid as the processing medium and are mainly restricted to wet processing methods such as casting/evaporation, which has been extensively used. The main advantage of this strategy relies in the fact that it allows preserving the dispersion state of the nanoparticles in the liquid. However, it limits the number of polymer matrices that can be used in association with cellulose nanoparticles. Moreover, this procedure is both nonindustrial and non-

Received: March 24, 2014
Accepted: May 19, 2014
Published: May 19, 2014

   dx.doi.org/10.1021/am501755p | ACS Appl. Mater. Interfaces 2014, 6, 9365−9375

economic. The next challenge consists most probably in the possibility of preparing polymer nanocomposites using industrial melt processing techniques, thus avoiding the liquid medium methods. Few solutions have been proposed to address this challenge. A glance at literature allows discerning different strategies. Polar matrices, such as starch[19] or poly(ethylene oxide) (PEO),[20] have been used. For apolar matrices, the use of solvent mixture or solvent exchange,[21−24] as well as different processing aids[25,26] were also reported. Melt compounding with chemically grafted nanoparticles was also reported.[27−30]

Among these different strategies, only chemical grafting was effective in dispersing the nanoparticles within the polymeric matrix by melt processing. However, it involves an additional step (chemical modification) that may be prohibitive for some applications.

We recently reported preliminary results regarding a simple method easily applicable at the industrial scale based on a physical compatibilization approach.[31] The basic idea consisted in wrapping the nanoparticles with a polymer bearing moieties susceptible to interact physically with the cellulosic surface and with an apolar matrix. We also showed that physical interaction of the polymer was enhanced when chemically grafting the same polymer on the surface of the nanoparticles.[32] This concept is investigated in more detail in the present paper. Nanocrystals extracted from two different cellulosic sources were used to evaluate the effect of the specific surface area of nanorod particles and the effect of starch nanocrystals with a plateletlike morphology was also investigated.

MATERIALS AND METHODS

Materials. Poly(ethylene oxide) (PEO) (Sigma-Aldrich) with different average molecular weights, viz. $M_w = 5 \times 10^6$ g mol^{-1}, 1×10^6 g mol^{-1}, 1×10^5 g mol^{-1}, 35×10^3 g mol^{-1}, 3.4×10^3 g mol^{-1}, and 1.5×10^3 g mol^{-1}, have been used in this study. They were labeled as 5, 1, 0.1, 0.035, 0.0034, and 0.0015 M, respectively, throughout the manuscript. It is well-known that PEO tends to refer to polymers with a molecular weight above 20 000 g mol^{-1}, whereas for oligomers and polymers with a molecular weight below 20 000 g mol^{-1} poly(ethylene glycol) (PEG) is used. However, for sake of clarity PEO was used regardless the molecular weight. Low density polyethylene (LDPE - Lacqtene 1008 FE 24) with a density of 0.924 g cm^{-3} was supplied by Atofina S.A.

Two different natural fibers have been used in this study to prepare cellulose nanocrystals (CNCs), viz. bleached cotton fibers (*Gossypium* sp.) and native capim dourado fibers from the Jalapão region, Tocantins State, Brazil. Sulfuric acid (≥95 wt %) was used as purchased from Aldrich. Native starch granules were kindly provided by Cargill (Krefeld, Germany) as waxy maize starch (C*Gel 04201, 98% amylopectin).

Preparation of PEO Solutions. Polymer solutions were obtained by adding the proper amount of PEO in distilled water (1.25 wt %) and mechanical stirring at room temperature. The solution was protected against light by an aluminum foil to prevent photo-oxidation of the polymer and weakly stirred at 500 rpm for 1−4 days, depending on the molecular weight. Solutions were then stored in darkness at 4 °C.

Preparation of Cellulose Nanocrystals (CNCs). Colloidal suspensions of CNCs in water were prepared from cotton linter as described elsewhere.[33,34] The cotton linter was milled with a laboratory milling device to obtain fine particulate substance. The cotton fibers were extracted in a 2 wt % aqueous NaOH solution for 12 h at room temperature under mechanical stirring and then filtered and rinsed with distilled water. Acid hydrolysis was done using 65 wt % aqueous sulfuric acid solution (11 wt % cotton fiber). The resulting suspension was held at 45 °C under mechanical stirring for 45 min to allow fibers hydrolysis.

For capim dourado, an exhaustive pretreatment of the fibers was performed as reported elsewhere.[35] Unbleached fibers were cut with a FRITSCH Pulverisette mill, until fine particulate fibers were obtained. Then, the fibers were treated with a 4 wt % aqueous NaOH solution for 2 h at 80 °C under mechanical stirring. This treatment was done in triplicate, in order to purify cellulose by removing other constituents present in the fiber. After each treatment, the material was filtered and washed with distilled water until the alkali was completely eliminated. A subsequent bleaching treatment was carried out to whiten the fibers. The solution used in this treatment was made by equal parts of acetate buffer, aqueous chlorite (1.7 wt % in water) and distilled water. The bleaching treatment was performed for 2 h at 80 °C under mechanical stirring and was repeated 4 times. After each treatment the fibers were filtered on a filter tissue (20 μm) and washed with distilled water. The acid hydrolysis treatment was achieved using 65 wt % aqueous sulfuric acid solution (preheated) under mechanical stirring. The fiber content was in the range 4−6 wt %. The resulting suspension was held at 45 °C under mechanical stirring for 75 min to allow fibers hydrolysis.

After hydrolysis, the ensuing suspensions were diluted with ice cubes or cold distilled water to stop the reaction and washed until neutrality by successive centrifugations at 10 ,000 rpm at 10 °C for 10 min each step and dialyzed against distilled water. Afterward the CNC suspensions were homogenized with an Ultra Turax T25 homogenizer for 5 min and the CNC dispersion was completed by an ultrasonic treatment using a Branson sonifier for four 5 min cycles (with cooling as necessary to prevent overheating). The suspensions were then filtered over no. 1 fritted glass filter in order to remove residual aggregates. The resulting suspensions were subsequently stored at 4 °C after adding several drops of chloroform in order to avoid bacterial growth until used.

Preparation of Starch Nanocrystals (SNC). The hydrolysis process developed by Angellier et al.[36] was used and slightly modified for preparing nanocrystals from starch. Briefly, 147 g of native starch was mixed with 1 L of previously prepared diluted sulfuric acid (3 M). The suspension was kept under 400 rpm mechanical stirring at 40 °C, using a silicon oil bath, for 5 days. The final suspension was washed by successive centrifugations in distilled water until reaching neutral pH and redispersed using Ultra Turrax for 5 min at 13,000 rpm to avoid aggregates. The obtained suspension was filtered on a filter tissue (40 μm, ref 03−41/31 Buisine, France).

Determination of CNC and SNC Content in Suspensions. To ascertain the nanocrystal content in the aqueous suspensions, samples of known weight were left to air-dry into films over 2−3 days. Once dry, the samples were then reweighed and the weight percent was calculated as a percentage of the initial amount. In this research, three samples were tested to ensure accuracy in the result.

Surface Modification of Nanocrystals with PEO. After the aqueous PEO solutions were prepared, i.e., the polymer was fully dispersed, known quantities of CNC or SNC in aqueous suspension form were added ranging from 0 wt % to 9 wt % (dry content of nanoparticles based on PEO amount). Then distilled water was added to ensure the resulting suspension had an overall PEO concentration of 1 wt %. So, through the addition of known quantities of nanocrystal suspensions and water, suspensions containing 1 wt % PEO and $0-9 \times 10^{-2}$ wt % CNC or SNC (actual overall concentration) were prepared.

Processing of Nanocomposite Materials. Nanocomposite materials were prepared by mixing LDPE and either unmodified or PEO-modified CNC or SNC (nanoparticle content ranging from 0 to 9 wt % based on LDPE content) using a twin-screw DSM Micro 15 compounder. For PEO-modified nanoparticles 50:50 PEO:nanoparticle suspensions were used. The suspensions were freeze-dried before extrusion. The components were introduced in the mixing chamber and allowed to melt at 160 °C. The mixing speed was set at 60 rpm for 10 min and extrusion was carried out with a slit die 0.6 mm in width and 1 cm in length.

Characterization. *Microscopies.* Micrographs of cotton CNC were taken with a ZEISS-ULTRA55 field emission gun scanning electron microscope (FEG-SEM) with an acceleration voltage of 15 kV. Nanoparticles were deposited from a droplet of a dilute suspension on a microgrid (200 mesh, Electron Microscopy Sciences, Hatfield, PA, USA).

Atomic Force Microscopy (AFM) observations were performed on a Multimodal AFM (DI, Veeco, Instrumentation Group) with both tapping and conductive mode (C-AFM). The tips were Multi130 for

tapping and MESP for C-AFM. A drop of SNC or CNC suspension was deposited on a mica substrate (split with adhesive tape) and dried for few minutes at 40 °C. Between 30 and 110 measurements were used depending on the source to determine the average thickness and standard deviation.

Rheometry. The rheometrical measurements were performed using a rotational rheometer, the DHR3 from TA Instrument. Cone−plate geometry, with a 60 mm diameter plate and a cone angle of 0.995°, was used. The geometry was enclosed in a solvent trap allowing the saturation of the atmosphere and thus preventing from solvent evaporation. A Peltier thermoelectric device was used to keep the sample at the desired temperature of 20 °C during the experimental runs.

The rheometrical tests were based first on dynamic measurements using small amplitude oscillatory shear deformations. This allow to measure the elastic and viscous modulus, G' and G'', as a function of the frequency of the oscillations ω. Oscillatory measurements were performed under linear viscoelastic conditions. These were determined under strain sweep experiments at a fixed frequency. The strain range varies from 0.1% to 100%. The frequencies used are fixed at 1, 10, and 100 Hz. Then, isothermal frequency sweeps are carried out within the linear viscoelastic regime and the elastic and viscous modulus measured. The complex viscosity $\eta^*(\omega)$ is deduced from those measurements.

Steady state measurements were also performed to determine the variation of the shear viscosity as a function of the shear rate. To do so, transient flows were performed at different shear rates, ranging from 3×10^{-3} to 1 s^{-1}, and the steady-state viscosity values were determined as the plateau value obtained at long-time scales of the transient viscosity.

X-ray Diffraction. X-ray diffraction data were recorded in reflection mode for dry nanoparticle powders at room temperature with a Siemens D500 diffractometer operated at 30 kV and 20 mA, and equipped with a CuKα anode (λ = 0.154 nm). Diffraction patterns were obtained in the range 2θ = 5−55° using a fixed time mode with a step interval of 0.02°.

Thermal Analysis. Thermogravimetric analysis (TGA) (STA 6000, PerkinElmer Instruments model, USA) was carried out to determine the thermal stability of samples in a nitrogen atmosphere (20 mL min^{-1}). The samples were heated from 30 to 600 °C with a heating rate of 10 °C min^{-1}. The sample weight was plotted as a function of temperature for all samples.

Differential scanning calorimetry (DSC) experiments were performed on LDPE based nanocomposites with a DSC Q100 differential scanning calorimeter (TA Instruments, USA) fitted with a manual liquid nitrogen cooling system. Samples with weight ranging between 6 and 10 mg were sealed in aluminum pans and placed in the DSC cell in glovebox under nitrogen atmosphere to minimize the oxidative degradation. The heating and cooling steps were carried out from −100 to 150 °C and from 150 °C to −100 °C, respectively, at a rate of 10 °C min^{-1}. The melting temperature (T_m) was taken as the peak temperature of the melting endotherm, while the heat of fusion was calculated from the area of the peaks. The degree of crystallinity (χ_c) was determined from DSC thermograms using the relationship

$$\chi_c = \frac{\Delta H_m}{w \Delta H_m^\circ} \quad (1)$$

where ΔH_m° = 290 J g^{-1} was taken for 100% crystalline LDPE and w is the weight fraction of LDPE matrix in the nanocomposite.

Tensile Tests. The nonlinear mechanical properties of the composites were analyzed under controlled ambient conditions (25 °C and 50% RH) using an Instron Universal Testing Machine model 4301 with a 100 N load cell, and with a crosshead speed of 10 mm min^{-1}. The samples were prepared by cutting strips 15 cm long and 2 cm wide from the extruded films, whereas the thickness was measured before each test. The distance between jaws was 10 cm. The stress−strain curves were plotted and the tensile modulus was deduced from the low strain region. The ultimate strength (σ_b) and elongation at break (ε_b) were also calculated. At least five specimens were tested to characterize each set of LDPE-based nanocomposites and the mean values were reported.

RESULTS AND DISCUSSION

Nanoparticle Characterization. Figure 1a shows an electron micrograph of cotton CNC. The average diameter and length of rod-like nanoparticles were calculated using digital image analysis. At least 100 measurements were carried out for both diameter and length. The average diameter (D) and length (L) of cotton CNC were approximately 11.16 ± 4.42 nm and 168.43 ± 58.34 nm, respectively, and the average aspect ratio (L/D) was around 15. It is close to values reported in literature for flax,[36] curaúa,[37] and kenaf[38] CNC. AFM image of CNC extracted from capim dourado is shown in Figure 1b. Much longer and thinner nanorods were observed with an average diameter and length around 4.5 ± 0.86 nm and 300 ± 93 nm, respectively, as reported elsewhere,[35] giving rise to an average aspect ratio around 67.

AFM image of SNC extracted from waxy maize starch is shown in Figure 1c. Platelet-like nanoparticles with lateral dimensions within 50−100 nm range were obtained as already reported for sulfuric acid-hydrolyzed waxy maize starch.[39,40]

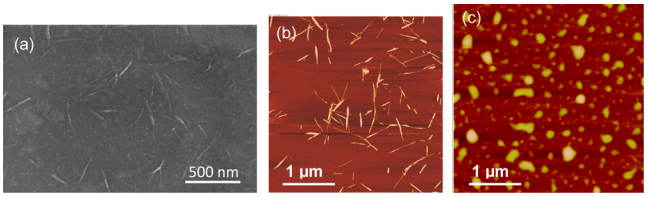

Figure 1. (a) FEG-SEM of a dilute suspension of CNC extracted from cotton, and AFM image of a dilute suspension of (b) CNC extracted from capim dourado and (c) SNC extracted from waxy maize starch.

Table 1. Average Length (L) and Diameter (D) for CNC Extracted from Cotton and Capim Dourado, Average Width (W) and Thickness (T) for SNC Extracted from Waxy Maize Starch, and Specific Surface Area (A_{sp})[a]

material	L (nm)	D (nm)	W (nm)	T (nm)	A_{sp} (m^2 g^{-1})
cotton CNC	168	11			242
capim dourado CNC	300	4.5			593
waxy maize SNC			75	6	258

[a] A_{sp} was estimated from these geometrical characteristics, assuming a density of 1.5 g cm^{-3} for crystalline cellulose and starch.

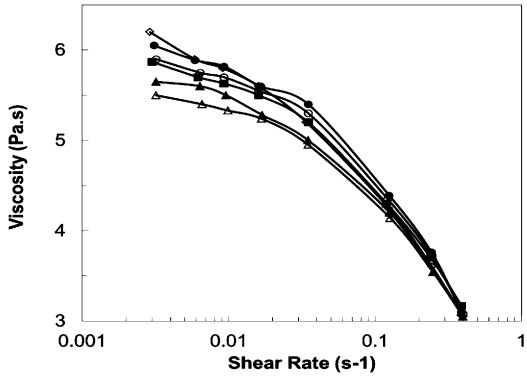

Figure 2. Evolution of the steady shear viscosity for the 1 wt % PEO (5 M, $M_w = 5 \times 10^6$ g mol^{-1}) solution containing various amounts of CNC extracted from capim dourado (on the PEO basis) as a function of the shear rate: 0 wt % (●), 3 wt % (○), 5 wt % (▲), 7 wt % (△), 9 wt % (■), and 11 wt % (◊). The solid lines serve to guide the eye.

dx.doi.org/10.1021/am501755p | ACS Appl. Mater. Interfaces 2014, 6, 9365−9375

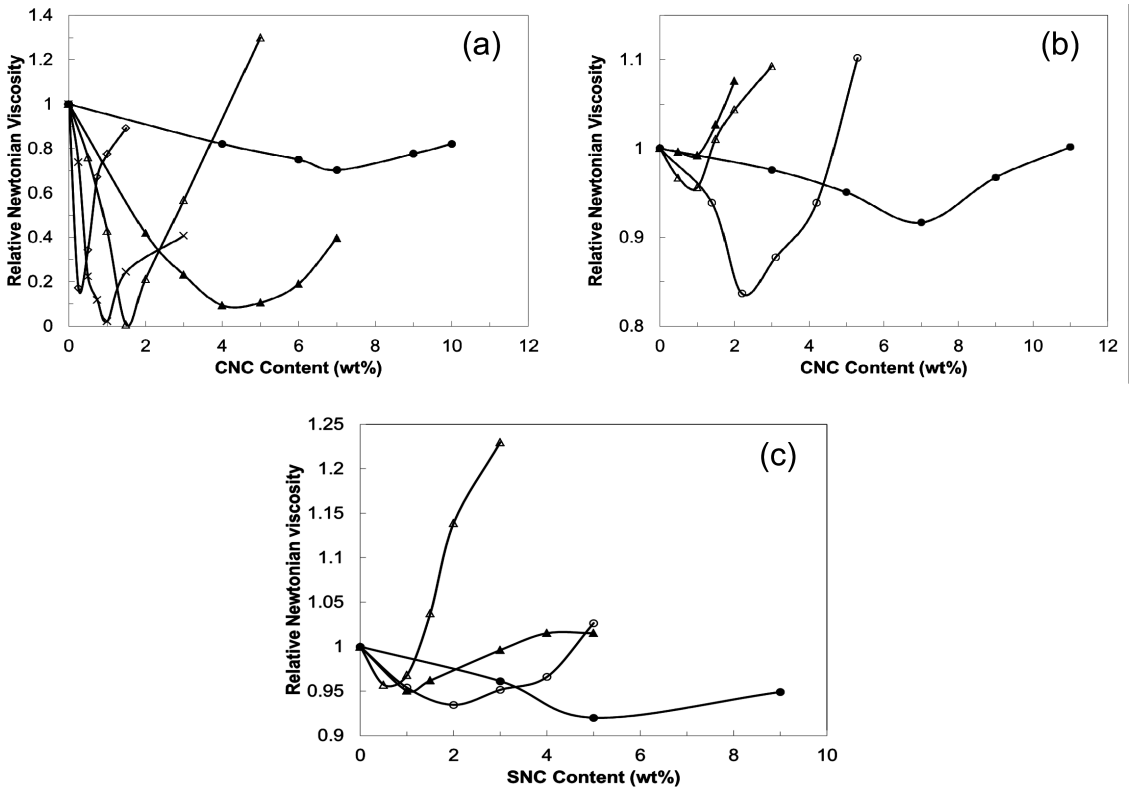

Figure 3. Evolution of the Newtonian steady shear viscosity for the 1 wt % solution containing various amounts of CNC (on the PEO basis) extracted from (a) cotton, (b) capim dourado, and (c) SNC extracted from waxy maize starch, as a function of the nanoparticle content: PEO 5 M (●), 1 M (○), 0.1 M (▲), 0.035 M (Δ), 0.0034 M (×), and 0.0015 M (◊). The solid lines serve to guide the eye.

Table 2. Number of PEO Chains Necessary to Saturate the Surface Unit of the Nanoparticles (N_{PEO}) and Corresponding Mass (W_{PEO}) for CNC Extracted from Cotton and Capim Dourado, and SNC Extracted from Waxy Maize Starch Calculated for the Different Molecular Weight PEOs

nanoparticle	M_w PEO (g mol^{-1})	C_{mini} (wt %)	N_{PEO} (chain m^{-2})	W_{PEO} (mg m^{-2})
cotton CNC	5×10^6	0.070	7.11×10^{15}	59
	1×10^5	0.042	5.92×10^{17}	98
	35×10^3	0.015	3.32×10^{16}	275
	3.4×10^3	0.010	4.98×10^{16}	413
	1.5×10^3	0.003	5.53×10^{20}	1377
capim dourado CNC	5×10^6	0.069	2.94×10^{15}	24
	1×10^6	0.023	4.41×10^{16}	73
	1×10^5	0.010	1.02×10^{18}	169
	35×10^3	0.009	3.22×10^{18}	187
waxy maize SNC	5×10^6	0.050	9.33×10^{15}	78
	1×10^6	0.020	1.17×10^{17}	194
	1×10^5	0.010	2.33×10^{18}	388
	35×10^3	0.006	1.11×10^{19}	646

Geometrical characteristics as well as a rough estimate of the specific surface areas (A_{sp}) calculated from these dimensions and assuming a density (ρ) of 1.5 g cm^{-3} for crystalline cellulose and starch are collected in Table 1. For rodlike CNC, the surface of the ends of the rods was neglected and the A_{sp} values were calculated from

$$A_{sp} = \frac{4}{\rho D} \quad (2)$$

where D is the diameter of the rod. For waxy maize SNC, dimensions were estimated as 50−100 nm (average value 75 nm) for the width (W) as observed by AFM, and 5−7 nm (average value 6 nm) for thickness (T) as reported elsewhere.[41] The following equation was used to calculate the specific surface area of SNS

$$A_{sp} = \frac{2}{\rho}\left(\frac{1}{T} + \frac{2}{W}\right) \quad (3)$$

Rheological Measurements. In our preliminary report,[31] it was shown that adding CNC to a high molecular weight PEO solution resulted in a decrease of the viscosity of the mixture followed by an increase. Favorable interaction between PEO chains and surface of the nanoparticles were suspected. It is now of interest to see the influence of both the molecular weight of PEO chains and specific surface area of the nanoparticles on this phenomenon. Rheological measurements were performed for the three different nanoparticles (CNC from cotton and capim dourado, and waxy maize SNC) and PEO with different molecular weights. A typical plot showing the evolution of the steady shear viscosity for the 1 wt % PEO (5 M, $M_w = 5 \times 10^6$ g mol^{-1}) solution containing various amounts of CNC extracted from capim dourado (on the PEO basis) as a function of the shear rate is shown in Figure 2. All solutions/suspensions exhibit a low-shear Newtonian viscosity, followed by a shear thinning behavior. Even if the curves did not clearly show stabilization at low shear rate, the beginning of the Newtonian plateau is still observed. The viscosity values at very low shear rate have been used to estimate the Newtonian shear viscosity values.

Figure 3 shows the evolution of the relative Newtonian viscosity, i.e., ratio of the viscosity of the suspension to the one of

dx.doi.org/10.1021/am501755p | ACS Appl. Mater. Interfaces 2014, 6, 9365−9375

Figure 4. Appearance of freeze-dried cotton CNC samples consisting of (A) unmodified CNC, and a 50:50 mixture using (B) PEO 0.0015 M, (C) PEO 0.0034 M, (D) PEO 0.035 M, (E) PEO 0.1 M, and (F) PEO 5 M.

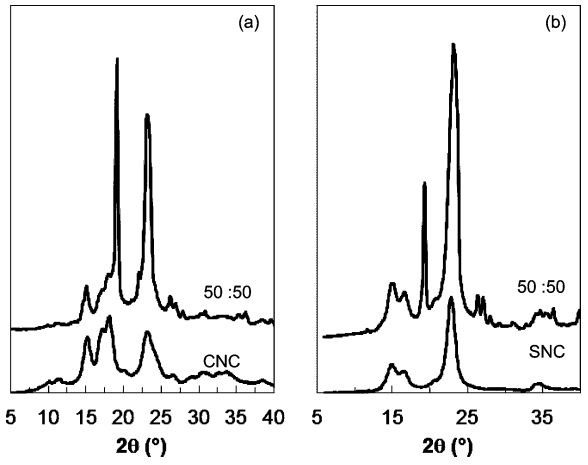

Figure 5. X-ray diffraction patterns of (a) cotton CNC: unmodified CNC and 50:50 mixture with PEO 5 M, and (b) waxy maize SNC: unmodified SNC and 50:50 mixture with PEO 5 M.

the nanoparticle-free PEO solution, for the different systems as a function of nanoparticle content. As reported previously[31] for cotton CNC/PEO 5M, the viscosity first decreases upon adding nanoparticles and then increases for higher filler contents showing a minimum viscosity value for a critical nanoparticle loading level. The initial decrease in viscosity was attributed to strong affinity between PEO chains and the cellulosic surface through interactions between the oxygen groups of PEO and hydroxyl groups of cellulose. Similar interactions obviously occurred for starch. The affinity of water to cellulose/starch surface as a competitive binder is higher, but the polymeric nature of PEO and possibility of wrapping have to be considered. Consequently, increasing nanoparticle content leads to an increase of the available specific area, and less free PEO chains are available in the solution. Interactions between the nanoparticles are hidden, and the behavior is close to that of water. When the nanoparticle is saturated with the PEO chains available in the suspension the viscosity displays the minimum value corresponding therefore to a critical concentration. Above this critical value, the viscosity increases with filler content, and the suspension displays a typical suspension behavior with a viscosity increasing with the suspension concentration.

The same behavior was observed for all nanoparticles and all PEOs but interestingly, the minimum viscosity occurred for filler content all the lower than the PEO molecular weight was low. CNC/PEO interactions were characterized and quantified using heat flow microcalorimetry.[9] Significant interactions between ether oxygen groups of PEO and the cellulosic surface were observed but stronger affinity of the CNC surface with hydroxyl end groups of POE than its ether oxygen groups was reported. This is most probably the reason why the viscosity of the suspension reaches a minimum value for lower nanoparticle content when using lower-molecular-weight PEO.

From the specific surface area of the nanoparticles and characteristics of the PEO chains, both the number of chains and the weight of PEO interacting with the surface unit of the nanoparticle can be calculated. The number of PEO chains necessary to saturate the surface unit of the nanoparticles (N_{PEO}) can be calculated from the following equation:

$$N_{PEO} = \frac{N_A}{M_{PEO} C_{mini} A_{sp}} \quad (4)$$

where N_A is the Avogadro number, M_{PEO} the average molecular weight of PEO, and C_{mini} the weight fraction of nanoparticle corresponding to the minimum value of the viscosity. The associated mass of PEO (W_{PEO}) can be calculated from

$$W_{PEO} = \frac{N_{PEO} M_{PEO}}{N_A} = \frac{1}{C_{mini} A_{sp}} \quad (5)$$

The N_{PEO} and W_{PEO} values for the different polysaccharide nanoparticles and PEO systems have been estimated and data are reported in Table 2. As expected, for a given nanoparticle, the amount of PEO chains interacting with the nanoparticle surface increases as the molecular weight of the polymer decreases. When comparing CNC extracted from cotton and from capim dourado with two very different specific surface areas, the amount of PEO chains interacting with the surface of the nanoparticle increases as A_{sp} decreases. Interestingly, much more PEO chains are able to interact with SNC surface than with CNC surface. The reasons for these observations are unclear now. This behavior is different from the results reported with fumed silica nanoparticles and PEO of different molecular weights where the surface coverage was obtained from adsorption measurements and this coverage was observed to increase with increasing chain length.[42]

Freeze-Dried Nanoparticle/PEO Mixtures. The next step was to take advantage of the favorable cellulose/PEO interactions to use the wrapping PEO chains as a compatibilizer to process nanocomposite films by extrusion. It could act as a

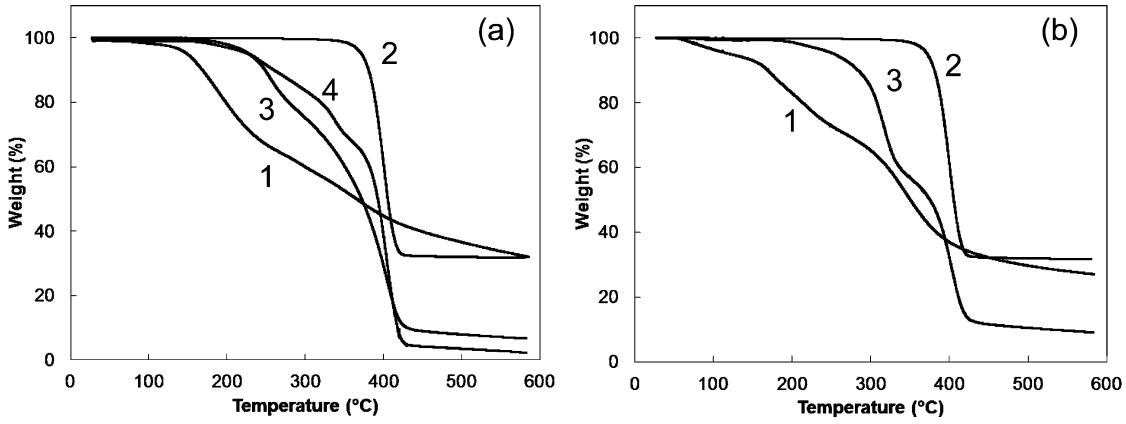

Figure 6. TGA curves of freeze-dried (a) cotton CNC: unmodified CNC (1), PEO 5 M (2), CNC:PEO 50:50 mixture with PEO 5 M (3), and CNC:PEO 50:50 mixture with PEO 0.035 M (4); and (b) waxy maize SNC: unmodified SNC (1), PEO 5 M (2), and SNC:PEO 50:50 mixture with PEO 5 M (3).

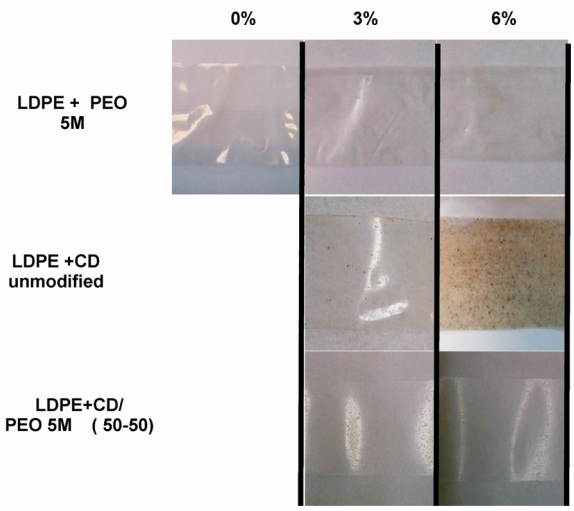

Figure 7. Pictures of the extruded films: LDPE-PEO 5 M blends (LDPE + PEO 5 M, PEO content ranging between 0 and 6 wt %), and LDPE reinforced with neat capim dourado CNC (LDPE + CD unmodified, CNC content of 3 and 6 wt %) and PEO 5 M-modified capim dourado CNC (LDPE + CD/PEO 5 M (50−50), CNC content of 3 and 6 wt %).

surfactant but can probably support the high shear rates involved during the extrusion process and then the compatibilizer should not be removed from nanoparticle surface and blended with the matrix. It was shown from rheological measurements that saturation of the cellulosic surface occurred for quite low nanocrystal contents compared to the amount of PEO. It is therefore difficult to use such nanoparticles because the amount of PEO introduced in the composite would be very high. Therefore, even if only part of the nanocrystal surface would be covered with PEO chains, it was decided to prepare suspensions consisting of 1 wt % PEO and 1 wt % nanocrystal in water. Therefore, the ratio of cellulose-to-PEO is 50 wt % for the mixture. Prior to extrusion the mixture was freeze-dried and characterized.

After freeze-drying, it was possible to observe how the physical appearance of the sample differs with increasing PEO molecular weight. A sample of unmodified nanocrystal was also freeze-dried for comparison. Samples based on cotton CNC can be seen in Figure 4. The unmodified CNCs (Figure 4A) form a fine white powder after freeze-drying. When mixed with PEO 0.0015 M (Figure 4B) and PEO 0.0034 M (Figure 4C) the lyophilizate also occurred as a white powder, similar to unmodified CNC. As the PEO molecular weight increases the aspect of the freeze-dried samples changes. The freeze-dried sample obtained for PEO 0.035 M (Figure 4D) forms a powdery substance when agitated, but retained the cube shape aspect it was frozen into before the freeze-drying process. In the case of PEO, 0.1 M and PEO 5 M samples (Figure 4E, F, respectively), the lyophilizate formed a dense, white, spongy substance. Both substances retained the cube shape that they had been frozen into prior to freeze-drying.

Table 3. Temperature of Fusion (T_m), Associated Heat of Fusion (ΔH_m) and Degree of Crystallinity (χ_c) for Extruded Neat LDPE and Polysaccharide Nanocrystal-Based Nanocomposites

filler	compatibilizer	filler content (wt %)	T_m (°C)	ΔH_m (J g^{-1})	χ_c
		0	120.8	108.4	0.37
cotton CNC		3	121.9	113.2	0.40
		6	121.5	124.9	0.46
		9	120.9	111.6	0.42
	PEO 5 M	3	119.7	103.5	0.38
		6	118.7	113.3	0.44
	PEO 1 M	3	119.3	98.8	0.36
		6	119.4	114.9	0.45
		9	119.3	105.1	0.44
	PEO 0.035 M	3	120.7	116.6	0.43
		6	117.7	116.5	0.46
		9	117.3	114.7	0.48
CD CNC		3	117.9	125.6	0.45
		6	119.0	119.1	0.44
	PEO 5 M	3	120.3	125.2	0.46
		6	118.3	122.9	0.48
waxy maize SNC		3	120.1	124.9	0.44
		6	120.9	119.7	0.44
		9	117.7	125.7	0.48
	PEO 5 M	3	120.8	129.4	0.47
	PEO 1 M	3	117.3	107.9	0.40
		6	119.9	113.9	0.45
		9	118.7	117.9	0.50
	PEO 0.035 M	3	117.9	115.3	0.42
		6	118.4	119.0	0.47
		9	118.3	122.5	0.52

dx.doi.org/10.1021/am501755p | ACS Appl. Mater. Interfaces 2014, 6, 9365−9375

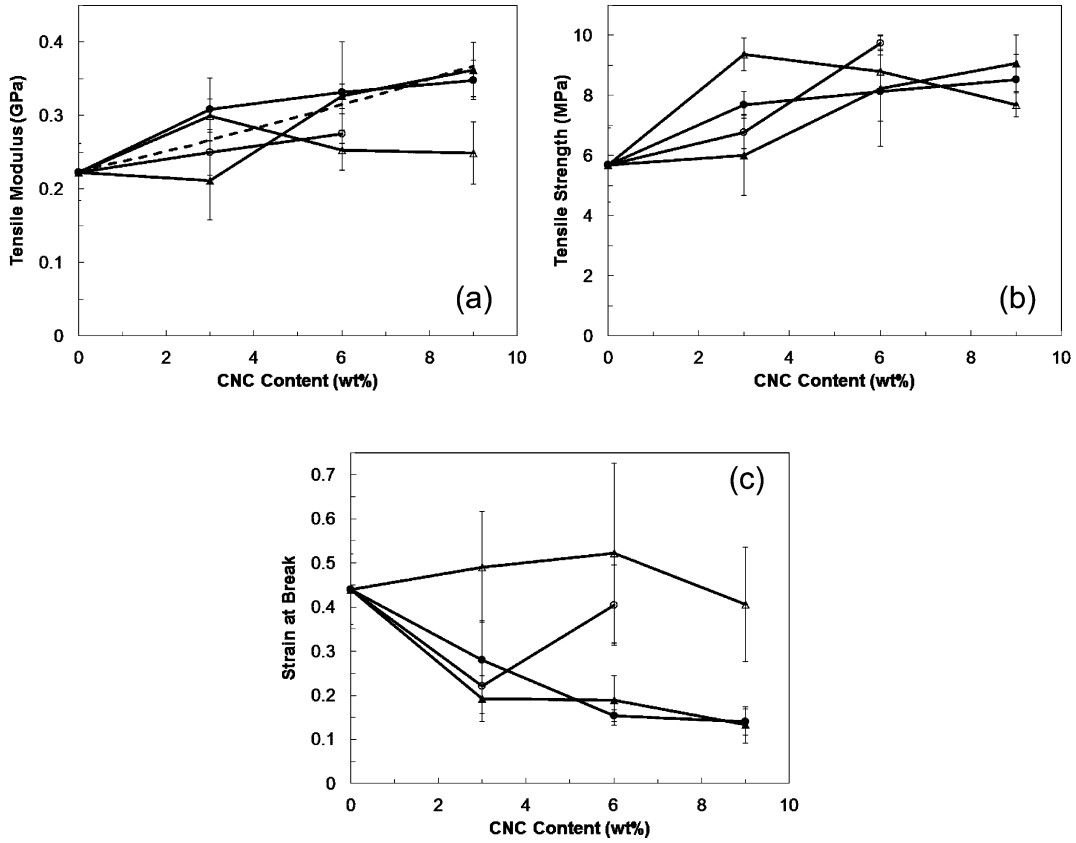

Figure 8. Evolution of (a) the tensile modulus, (b) tensile strength, and (c) elongation at break as a function of the cotton CNC content for nanocomposite films reinforced with unmodified CNC (●), PEO 5 M-modified CNC (○), PEO 1 M-modified CNC (▲), and PEO 0.035 M-modified CNC (Δ). The lines serve to guide the eyes. The dashed line in panel a corresponds to the prediction from the Halpin−Kardos model.

It was observed that both deformed semielastically upon applying a force, showing some spring-back.

The freeze-dried samples were characterized using X-ray diffraction. X-ray diffraction patterns obtained for cotton CNC (panel A) and waxy maize SNC (panel B) are shown in Figure 5. The pure CNC sample (Figure 5A) displays four well-defined peaks around 2θ = 14.5, 16.5, 22.5, and 34° typical of cellulose I. The hydrolyzed waxy maize starch nanoparticles (Figure 5B) show the expected scattering pattern for the A allomorph with the 18° (equator d spacing of 0.49 nm) signature peak, always found as a doublet with a signal at 17.2° (d = 0.52 nm) and at 23° (d = 0.39 nm).[43,44] There is also no signal at 5.5° (d = 1.16 nm), a signature signal for the B allomorph.[44] When freeze-dried with PEO 5 M, new characteristic prominent diffraction peaks appear around 19 and 23°, which are ascribed to PEO (Figure 5).

One of the main issues for the melt processing of acid-hydrolyzed polysaccharide nanocrystal reinforced nanocomposites is the thermal stability of the nanoparticles. TGA experiments were performed to investigate this property. Some data are reported in Figure 6. Panel a corresponds to cotton CNC-based materials. For neat CNC (curve 1), an initial weight loss is observed upon heating around 100 °C. It corresponds to the removal of moisture in the material. At higher temperatures, a gradual weight loss in the range 170−400 °C was reported. It is well-known that small amounts of sulfate groups resulting from the sulfuric acid hydrolysis process induce a considerable decrease in degradation temperatures.[45,46] A complex behavior was reported, in which the lower temperature degradation process may correspond to the degradation of more accessible and therefore more highly sulfated amorphous regions, whereas the higher temperature process is related to the breakdown of unsulfated crystal. The char fraction was also found to increase upon acid hydrolysis and displayed a continuous increase upon prolonged hydrolysis times.[45] It was ascribed to the higher amount of sulfated groups acting as flame retardants. PEO 5 M displayed a much higher thermal stability with a sharp weight loss within a narrow temperature range around 400 °C (curve 2). The char residue around 30% was similar to the one of neat CNC. This behavior was very similar regardless the molecular weight of PEO chains (results not shown).

The CNC:PEO mixture shows an intermediate behavior and an improved thermal stability was observed compared to unmodified CNC. The main degradation process was shifted toward higher temperatures and occurred in a narrower temperature range. This effect was enhanced when decreasing the molecular weight of PEO (curves 3 and 4 in Figure 6a). This is probably ascribed to a protection role of interacting PEO chains that hid the surface sulfate groups of CNC. Stronger interactions of low molecular weight PEO can explain the different behavior. Interestingly, the char residue was much lower than for pure components. A very similar behavior was observed for SNC (Figure 6b).

Polysaccharide Nanocrystal Reinforced LDPE. Both neat and PEO-modified freeze-dried nanoparticles were extruded with LDPE to prepare nanocomposite films. Figure 7 shows the aspect of extruded films composed of neat LDPE, LDPE-PEO blends (3 at 6 wt % PEO), as well as unmodified and PEO 5 M-modified capim dourado CNC reinforced LDPE. The neat LDPE film is obviously translucent as for any low thickness polymeric film with a relatively low degree of crystallinity

dx.doi.org/10.1021/am501755p | ACS Appl. Mater. Interfaces 2014, 6, 9365−9375

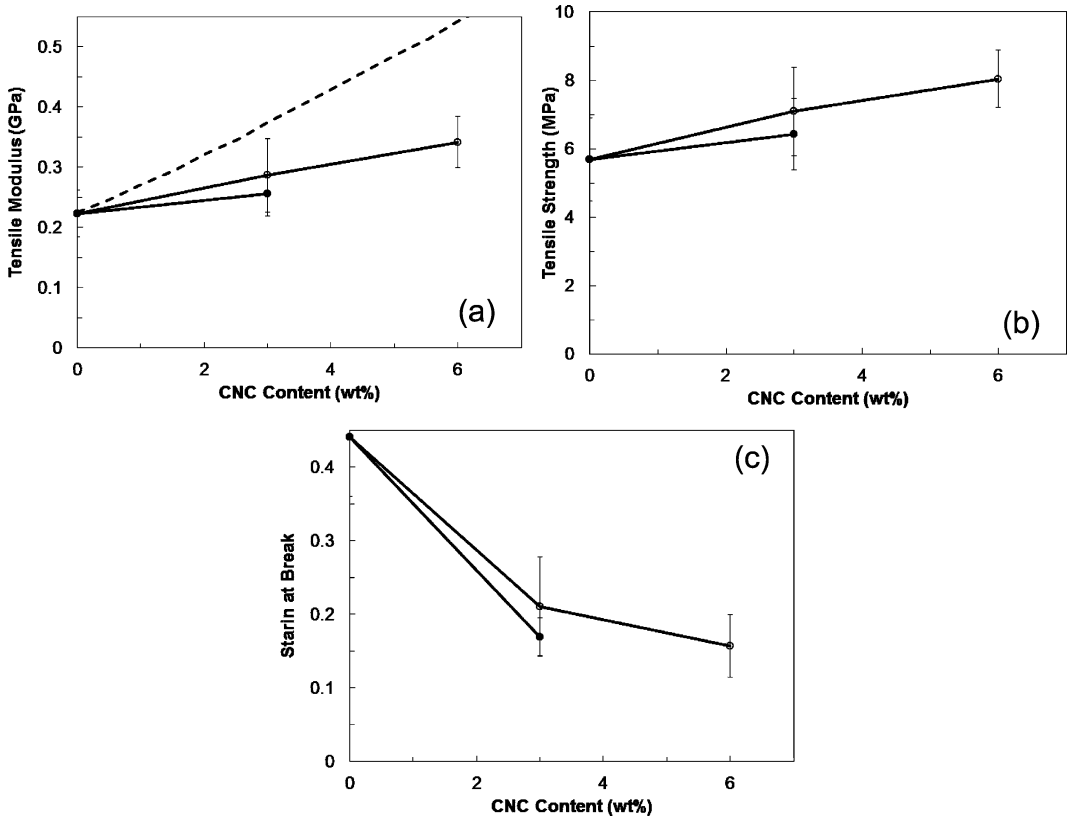

Figure 9. Evolution of (a) the tensile modulus, (b) tensile strength, and (c) elongation at break as a function of the capim dourado CNC content for nanocomposite films reinforced with unmodified CNC (●), and PEO 5 M-modified CNC (○). The lines serve to guide the eyes. The dashed line in panel a corresponds to the prediction from the Halpin−Kardos model.

induced by ramifications. The aspect of LDPE-PEO blends remains very similar. When adding 3 and 6 wt % capim dourado CNC, the film becomes brown and dots progressively appeared. These dark dots are obviously attributed to the cellulosic nanoparticles and reveal their degradation upon extrusion at 160 °C, as well as inhomogeneous dispersion within the polymeric matrix. It is ascribed to the low thermal stability of neat CNC evidenced from TGA experiments, and polar nature of cellulose inducing their self-aggregation when blended with a highly apolar polymer such as LDPE. The modification of CNC with PEO chains changes the aspect of the extruded nanocomposite films. Compared to the previous set of samples, they appeared much more homogeneous and less thermally degraded. The former observation can be ascribed to the compatibilizing role of PEO chains and the latter observation correlates with TGA experiments. Similar observations were reported for other nanocomposite films.

The thermal behavior of extruded nanocomposite films was characterized by DSC. The values of the melting temperature (Tm), enthalpy of fusion (ΔHm) and degree of crystallinity (χc) calculated using eq 1 are collected in Table 3. For the calculation of the degree of crystallinity, it is worth noting that the enthalpy of fusion was normalized to account for the effective LDPE content. No significant difference is reported for the melting point that ranges roughly between 117 and 122 °C regardless the filler content and PEO compatibilizer molecular weight. This is an indication that the crystallite size of LDPE is not significantly affected. Regarding the degree of crystallinity, the general trend is an increase upon nanofiller loading. This effect has been abundantly reported in literature for different polymeric matrices and is generally ascribed to a nucleating agent action of the dispersed phase. Similar results have been observed for LDPE films reinforced with neat and chemically modified CNC obtained by extrusion.[27] This nucleating effect was not influenced by the grafting of aliphatic chains at the nanoparticle surface.

The mechanical behavior of LDPE based nanocomposite films was investigated through tensile tests performed at room temperature. From the obtained stress−strain curves, the strength, tensile modulus and elongation at break for polysaccharide nanocrystal reinforced LDPE were determined. Figures 8−10 shows the evolution of these parameters as a function of the filler content for cotton CNC, capim dourado CNC, and waxy maize SNC, respectively. Globally, a weak increase of both the tensile modulus and tensile strength is observed upon nanoparticle addition. However, this increase is possibly due, at least partially, to the nanoparticle-induced crystallization of the LDPE matrix. The elongation at break decreases as the nanoparticle content increases, except for low molecular weight PEO-compatibilized systems, as for instance for PEO 0.035 M-modified cotton CNC (Figure 8c), and PEO 1 M- and PEO 0.035 M-modified SNC (Figure 10c). It could be attributed to improved dispersion induced by low molecular PEO.

The mechanical performance of extruded LDPE-based nanocomposites were very disappointing and very far from expectations based on some previous works.[6,7,9] However, it is worth noting that the outstanding mechanical properties reported in these earlier studies were ascribed not only to the high modulus and high aspect ratio of CNCs, but also to the formation of a percolating nanoparticle network. Slow wet processes such as casting/evaporation were reported to give the

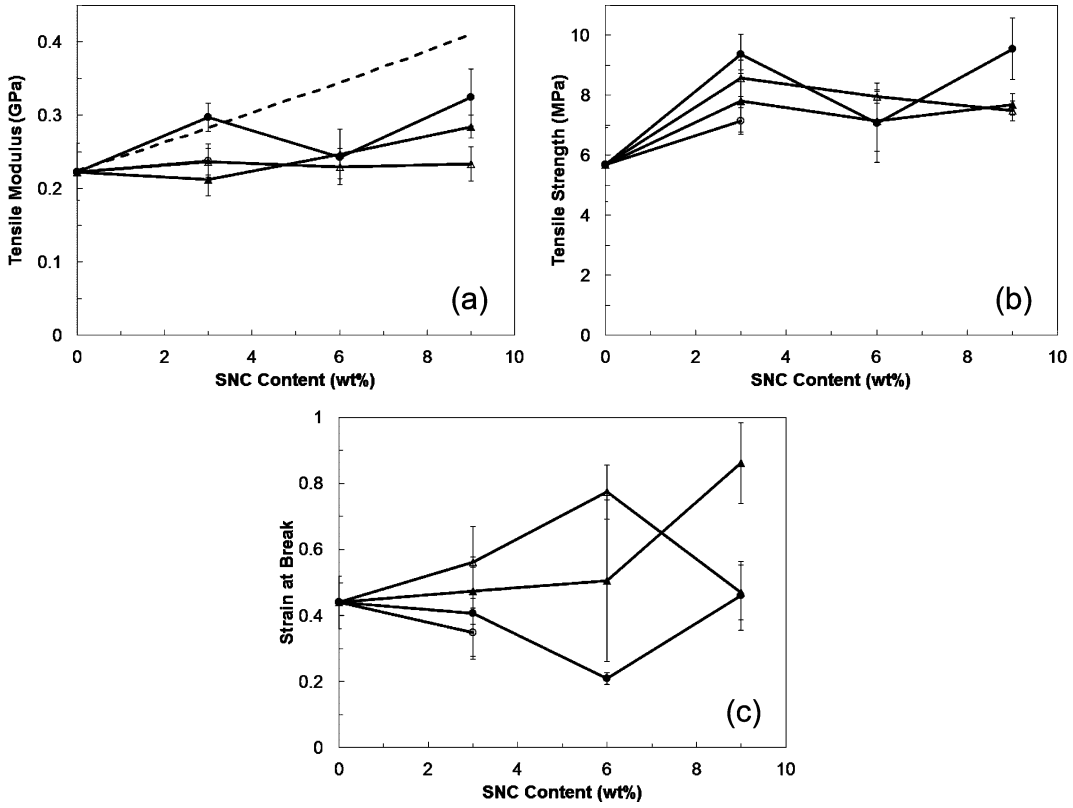

Figure 10. Evolution of (a) the tensile modulus, (b) tensile strength, and (c) elongation at break as a function of the waxy maize SNC content for nanocomposite films reinforced with unmodified SNC (●), PEO 5 M-modified SNC (○), PEO 1 M-modified SNC (▲), and PEO 0.035 M-modified SNC (Δ). The lines serve to guide the eyes. The dashed line in panel (a) corresponds to the prediction from the Halpin−Kardos model.

highest mechanical performance materials compared to other processing techniques. Indeed, during liquid evaporation strong interactions between nanoparticles can settle and promote the formation of a strong percolating network through hydrogen bonding forces. In this case comparison between experimental data and predicted values calculated from the percolation approach can be used to ensure that good dispersion and effective percolation occur. It corresponds to the highest mechanical properties that can be reached for a given polymeric system.

Such a percolation phenomenon is hindered in the present systems for several reasons:

(1) Extrusion involves high shear rates that would prevent the formation of the network.
(2) Aggregation of the nanocrystals occurs, at least for unmodified nanoparticles.
(3) Even for modified nanoparticles for which an improved dispersion was observed, their coating with PEO prevents direct interactions between the nanoparticles.

For these reasons, the only possible reinforcing capability of the nanocrystals to the LDPE matrix originates from their intrinsic mechanical properties. Then, we predicted the mechanical properties of the LDPE extruded nanocomposite materials from a mean field approach (Halpin-Kardos model) that assumes no interactions between the nanocrystals (details in the Supporting Information). The predicted data for the tensile modulus are reported as dashed lines in Figures 8a, 9a, and 10a. For cotton CNC based nanocomposites (Figure 8a) a good agreement was observed between experimental and predicted data. For capim dourado cellulose nanocrystal reinforced LDPE (Figure 9a), the predicted data were higher than experimental. A possible explanation for this discrepancy is related to the higher aspect ratio of these nanorods compared to cotton CNC that makes them more sensitive to breaking during the extrusion process. Indeed, a decrease in the length but also cross-section upon extrusion with PEO was reported for ramie CNC which decreased their aspect ratio from 28 to 24.[20] It was also shown that longer nanocrystals were more efficiently degraded leading to a significant narrowing of the length distribution. Therefore, a lower average length value than the one obtained from microscopic observation before extrusion should have been used in the prediction to properly describe the experimental behavior. For SNC-based nanocomposites (Figure 10a), a better agreement between experimental and predicted data was observed but not as good as for cotton CNC. However, it is worth noting that for SNC the mechanical properties of cellulose crystal have been used for starch crystal because of the absence of experimental data for starch.

■ CONCLUSIONS

Nanocrystals with a rodlike shape but with different dimensions and specific surface area were prepared by acid hydrolysis of cotton and capim dourado cellulose, and with a plateletlike morphology by acid hydrolysis of waxy maize starch granules. These nanoparticles were progressively added to aqueous solutions of poly(ethylene oxide) (PEO) and the rheological behavior of ensuing suspensions was investigated. For all systems under study, a progressive decrease in the viscosity was observed upon nanoparticle addition up to a critical nanocrystal content after which the viscosity started to increase. This phenomenon evidenced strong interactions between PEO chains and nano-

particle surface. The critical nanocrystal content corresponding to the minimum viscosity value decreased as the molecular weight of PEO decreased because of stronger affinity of hydroxyl end groups of PEO with the polysaccharide than its ether oxygen groups. These specific interactions have been exploited to obtained PEO-coated nanoparticles upon freeze-drying thus avoiding their extensive self-aggregation. Ensuing nanoparticles have been used to prepare nanocomposites following a masterbatch preparation with a low density polyethylene (LDPE) matrix by melt extrusion. Improved dispersibility and reduced thermal degradation of the nanoparticles were observed showing the compatilizing action of PEO. A weak increase of the degree of crystallinity was observed for nanocomposites. Disappointing mechanical properties were reported for the nanocomposites that were globally well predicted from the Halpin−Kardos model evidencing the absence of interactions between the nanoparticles for the construction of a load-bearing structure. It raised the issue and challenge consisting in promoting the homogeneous melt dispersion of the polysaccharide nanoparticles and avoiding agglomeration during processing, thus requiring favorable filler/matrix interactions, and at the same time promoting filler/filler interactions to allow the beneficial formation of a percolating network of nanoparticles. These two requirements are simply conflicting and no suitable strategy has been proposed so far.

■ ASSOCIATED CONTENT

Supporting Information

Details for the modeling of the mechanical behavior of the nanocomposites using the theoretical model of Halpin−Kardos are provided. This material is available free of charge via the Internet at http://pubs.acs.org.

■ AUTHOR INFORMATION

Corresponding Author

*E-mail: alain.dufresne@pagora.grenoble-inp.fr.

Notes

The authors declare no competing financial interest.

■ ACKNOWLEDGMENTS

The authors thank the PolyNat Carnot Institute and CNRS for funding this project (Contract CARN 007-01).

■ REFERENCES

(1) Dufresne, A. *Nanocellulose: From Nature to High Performance Tailored Materials*; Walter de Gruyter GmbH: Berlin/Boston, 2012.

(2) Azizi Samir, M. A. S.; Alloin, F.; Dufresne, A. A Review of Recent Research into Cellulosic Whiskers, Their Properties and Their Application in Nanocomposite Field. *Biomacromolecules* **2005**, *6*, 612−626.

(3) Eichhorn, S. J.; Dufresne, A.; Aranguren, M.; Marcovich, N. E.; Capadona, J. R.; Rowan, S. R.; Weder, C.; Thielemans, W.; Roman, M.; Renneckar, S.; Gindl, W.; Veigel, S.; Keckes, J.; Yano, H.; Abe, K.; Nogi, N.; Nakagaito, A. N.; Mangalam, A.; Simonsen, J.; Benight, A. S.; Bismarck, A.; Berglund, L. A.; Peijs, T. Review: Current International Research into Cellulose Nanofibres and Nanocomposites. *J. Mater. Sci.* **2010**, *45*, 1−33.

(4) Moon, R. J.; Martini, A.; Nairn, J.; Simonsen, J.; Youngblood, J. Cellulose Nanomaterials Review: Structure, Properties and Nanocomposites. *Chem. Soc. Rev.* **2011**, *40*, 3941−3994.

(5) Dufresne, A. Comparing the Mechanical Properties of High Performances Polymer Nanocomposites from Biological Sources. *J. Nanosci. Nanotechnol.* **2006**, *6*, 322−330.

(6) Favier, V.; Canova, G. R.; Cavaillé, J. Y.; Chanzy, H.; Dufresne, A.; Gauthier, C. Nanocomposites Materials from Latex and Cellulose Whiskers. *Polym. Adv. Technol.* **1995**, *6*, 351−355.

(7) Dufresne, A.; Kellerhals, M. B.; Witholt, B. Transcrystallization in Mcl-PHAs/Cellulose Whiskers Composites. *Macromolecules* **1999**, *32*, 7396−7401.

(8) Anglès, M. N.; Dufresne, A. Plasticized Starch/Tunicin Whiskers Nanocomposites. 1. Structural Analysis. *Macromolecules* **2000**, *33*, 8344−8353.

(9) Azizi Samir, M. A. S.; Alloin, F.; Sanchez, J.-Y.; Dufresne, A. Cellulose Nanocrystals Reinforced Poly(oxyethylene). *Polymer* **2004**, *45*, 4033−4041.

(10) Roohani, M.; Habibi, Y.; Belgacem, N. M.; Ebrahim, G.; Karimi, A. N.; Dufresne, A. Cellulose Whiskers Reinforced Polyvinyl Alcohol Copolymers Nanocomposites. *Eur. Polym. J.* **2008**, *44*, 2489−2498.

(11) Azizi Samir, M. A. S.; Alloin, F.; Sanchez, J. Y.; El Kissi, N.; Dufresne, A. Preparation of Cellulose Whiskers Reinforced Nanocomposites from an Organic Medium Suspension. *Macromolecules* **2004**, *37*, 1386−1393.

(12) Viet, D.; Beck-Candanedo, S.; Gray, D. Dispersion of Cellulose Nanocrystals in Polar Organic Solvent. *Cellulose* **2007**, *14*, 109−113.

(13) Van den Berg, O.; Capadona, J. R.; Weder, C. Preparation of Homogeneous Dispersions of Tunicate Cellulose Whiskers in Organic Solvents. *Biomacromolecules* **2007**, *8*, 1353−1357.

(14) Schroers, M.; Kokil, A.; Weder, C. Solid Polymer Electrolytes Based on Nanocomposites of Ethylene Oxide-Epichlorohydrin Copolymers and Cellulose Whiskers. *J. Appl. Polym. Sci.* **2004**, *93*, 2883−2888.

(15) Siqueira, G.; Bras, J.; Dufresne, A. Cellulose Whiskers vs. Microfibrils: Influence of the Nature of the Nanoparticle and its Surface Functionalization on the Thermal and Mechanical Properties of Nanocomposites. *Biomacromolecules* **2009**, *10*, 25−432.

(16) Capadona, J. R.; Van den Berg, O.; Capadona, L.; Schroeter, M.; Tyler, D.; Rowan, S. J.; Weder, C. A Versatile Approach for the Processing of Polymer Nanocomposites with Self Assembled Nanofibre Templates. *Nat. Nanotechnol.* **2007**, *2*, 765−769.

(17) Heux, L.; Chauve, G.; Bonini, C. Nonflocculating and Chiral-Nematic Self-Ordering of Cellulose Microcrystals Suspensions in Nonpolar Solvents. *Langmuir* **2000**, *16*, 8210−8212.

(18) Lin, N.; Huang, J.; Dufresne, A. Preparations, Properties and Applications of Polysaccharide Nanocrystals in Advanced Functional Nanomaterials: A Review. *Nanoscale* **2012**, *4*, 3274−3294.

(19) Orts, W. J.; Shey, J.; Imam, S. H.; Glenn, G. M.; Guttman, M. E.; Revol, J. F. Application of Cellulose Microfibrils in Polymer Nanocomposites. *J. Polym. Env.* **2005**, *13*, 301−306.

(20) Alloin, F.; D'Aprea, A.; Dufresne, A.; El Kissi, N.; Bossard, F. Poly(oxyethylene) and Ramie Whiskers Based Nanocomposites: Influence of Processing: Extrusion and Casting/Evaporation. *Cellulose* **2011**, *18*, 957−973.

(21) Iwatake, A.; Nogi, M.; Yano, H. Cellulose Nanofiber-Reinforced Polylactic Acid. *Compos. Sci. Technol.* **2008**, *68*, 2103−2106.

(22) Suryanegara, L.; Nakagaito, A. N.; Yano, H. The Effect of Crystallization of PLA on the Thermal and Mechanical Properties of Microfibrillated Cellulose-Reinforced PLA Composites. *Compos. Sci. Technol.* **2009**, *69*, 1187−1192.

(23) Suryanegara, L.; Okumura, H.; Nakagaito, A. N.; Yano, H. The Synergetic Effect of Phenylphosphonic Acid Zinc and Microfibrillated Cellulose on the Injection Molding Cycle Time of PLA Composites. *Cellulose* **2011**, *18*, 689−698.

(24) Jonoobi, M.; Harun, J.; Mathew, A. P.; Oksman, K. Mechanical Properties of Cellulose Nanofiber (CNF) Reinforced Polylactic Acid (PLA) Prepared by Twin Screw Extrusion. *Compos. Sci. Technol.* **2010**, *70*, 1742−1747.

(25) Bondeson, D.; Oksman, K. Polylactic Acid/Cellulose Whisker Nanocomposites Modified by Polyvinyl Alcohol. *Composites Part A* **2007**, *38*, 2486−2492.

(26) Fortunati, E.; Armentano, I.; Zhou, Q.; Iannoni, A.; Saino, E.; Visai, L.; Berglund, L. A.; Kenny, J. M. Multifunctional Bionanocompo-

site Films of Poly(Lactic Acid), Cellulose Nanocrystals and Silver Nanoparticles. *Carbohydr. Polym.* **2012**, *87*, 1596−1605.
(27) de Menezes, A. J.; Siqueira, G.; Curvelo, A. A. S.; Dufresne, A. Extrusion and Characterization of Functionalized Cellulose Whisker Reinforced Polyethylene Nanocomposites. *Polymer* **2009**, *50*, 4552−4563.
(28) Goffin, A.-L.; Raquez, J.-M.; Duquesne, E.; Siqueira, G.; Habibi, Y.; Dufresne, A. Dubois, Ph. Poly(ε-Caprolactone) Based Nanocomposites Reinforced by Surface-Grafted Cellulose Nanowhiskers via Extrusion Processing: Morphology, Rheology, and Thermo-Mechanical Properties. *Polymer* **2011**, *52*, 1532−1538.
(29) Goffin, A.-L.; Raquez, J.-M.; Duquesne, E.; Siqueira, G.; Habibi, Y.; Dufresne, A. Dubois, Ph. From Interfacial Ring-Opening Polymerization to Melt Processing of Cellulose Nanowhisker-Filled Polylactide-Based Nanocomposites. *Biomacromolecules* **2011**, *12*, 2456−2465.
(30) Raquez, J. M.; Murena, Y.; Goffin, A. L.; Habibi, Y.; Ruelle, B.; DeBuyl, F. Dubois, Ph. Surface-Modification of Cellulose Nanowhiskers and Their Use as Nanoreinforcers into Polylactide: A Sustainably-Integrated Approach. *Compos. Sci. Technol.* **2012**, *72*, 544−549.
(31) Ben Azouz, K.; Ramires, E. C.; Van den Fonteyne, W.; El Kissi, N.; Dufresne, A. Simple Method for the Melt Extrusion of a Cellulose Nanocrystal Reinforced Hydrophobic Polymer. *ACS Macro Lett.* **2012**, *1*, 236−240.
(32) Lin, N.; Dufresne, A. Physical and/or Chemical Compatibilization of Extruded Cellulose Nanocrystal Reinforced Polystyrene Nanocomposites. *Macromolecules* **2013**, *46*, 5570−5583.
(33) Dong, X. M.; Kimura, T.; Revol, J. F.; Gray, D. G. Effects of Ionic Strength on the Isotropic-Chiral Nematic Phase Transition of Suspensions of Cellulose Crystallites. *Langmuir* **1996**, *12*, 2076−2082.
(34) De Souza Lima, M. M.; Wong, J. T.; Paillet, M.; Borsali, R.; Pecora, R. Translational and Rotational Dynamics of Rodlike Cellulose Whiskers. *Langmuir* **2003**, *19*, 24−29.
(35) Siqueira, G.; Abdillahi, H.; Bras, J.; Dufresne, A. High Reinforcing Capability Cellulose Nanocrystals Extracted from *Syngonanthus nitens* (Capim Dourado). *Cellulose* **2010**, *17*, 289−298.
(36) Cao, X.; Dong, H.; Li, C. M. New Nanocomposite Materials Reinforced with Flax Cellulose Nanocrystals in Waterborne Polyurethane. *Biomacromolecules* **2007**, *8*, 899−904.
(37) Corrêa, A. C.; Teixeira, E. M.; Pessan, L. A.; Mattoso, L. H. C. Cellulose Nanofibers from Curaua Fibers. *Cellulose* **2010**, *17*, 1183−1192.
(38) Kargarzadeh, H.; Ahmad, I.; Zanariah Zainuddin, S. Y.; Abdullah, I.; Dufresne, A. Effect of Hydrolysis Conditions on the Morphology, Crystallinity and Thermal Stability of Cellulose Nanocrystals Extracted from Kenaf Bast Fibres. *Cellulose* **2012**, *19*, 855−866.
(39) Le Corre, D.; Bras, J.; Dufresne, A. Starch Nanoparticles: A Review. *Biomacromolecules* **2010**, *11*, 1139−1153.
(40) Namazi, H.; Dadkhah, A. Surface Modification of Starch Nanocrystals Through Ring-Opening Polymerization of ε-Caprolactone and Investigation of Their Microstructures. *J. Appl. Polym. Sci.* **2008**, *110*, 2405−2412.
(41) Putaux, J. L.; Molina-Boisseau, S.; Momaur, T.; Dufresne, A. Platelet Nanocrystals Resulting from the Disruption of Waxy Maize Starch Granules by Acid Hydrolysis. *Biomacromecules* **2003**, *4*, 1198−1202.
(42) Kawaguchi, M.; Yamamoto, T.; Kato, T. Rheological Properties of Silica Suspensions in Aqueous Solutions of Block Copolymers and Their Water-Soluble Components. *J. Colloid Interface Sci.* **2001**, *241*, 293−295.
(43) Matveev, Y. I.; van Soest, J. J. G.; Nieman, C.; Wasserman, L. A.; Protservo, V. A.; Ezernitskaja, M.; Yuryev, V. P. The Relationship Between Thermodynamic and Structural Properties of Low and High Amylose Maize Starches. *Carbohydr. Polym.* **2001**, *44*, 151−160.
(44) Katopo, H.; Song, Y.; Jne, J.-L. Effect and Mechanism of Ultrahigh Hydrostatic Pressure on the Structure and Properties of Starches. *Carbohydr. Polym.* **2002**, *47*, 233−244.
(45) Roman, M.; Winter, W. T. Effect of Sulphate Groups from Sulphuric Acid Hydrolysis on the Thermal Degradation Behaviour of Bacterial Cellulose. *Biomacromolecules* **2004**, *5*, 1671−1677.
(46) Lin, N.; Dufresne, A. Surface Chemistry, Morphological Analysis and Properties of Cellulose Nanocrystals with Gradient Sulfation Degrees. *Nanoscale* **2014**, *6*, 5384−5393.